# Impact of the Atlantic Meridional Overturning Circulation (AMOC) on Arctic Surface Air Temperature and Sea-Ice Variability

Salil Mahajan *

*Atmospheric and Oceanic Sciences Program, Princeton University, Princeton, New Jersey, USA*

Rong Zhang and Thomas L. Delworth

*Geophysical Fluid Dynamics Laboratory, Princeton, New Jersey, USA*

* *Corresponding author address:* Salil Mahajan, 300 Forrestal Road, Sayre Hall, Atmospheric and Oceanic Sciences Program, Princeton University, Princeton, New Jersey - 08544, USA

E-mail: smahajan@princeton.edu

ABSTRACT

The simulated impact of the Atlantic Meridional Overturning Circulation (AMOC) on the low frequency variability of the Arctic Surface Air temperature (SAT) and sea-ice extent is studied with a 1000 year-long segment of a control simulation of GFDL CM2.1 climate model. The simulated AMOC variations in the control simulation are found to be significantly anti-correlated with the Arctic sea-ice extent anomalies and significantly correlated with the Arctic SAT anomalies on decadal timescales in the Atlantic sector of the Arctic. The maximum anti-correlation with the Arctic sea-ice extent and the maximum correlation with the Arctic SAT occur when the AMOC Index leads by one year. An intensification of the AMOC is associated with a sea-ice decline in the Labrador, Greenland and Barents Seas in the control simulation, with the largest change occurring in the winter. The recent declining trend in the satellite observed sea-ice extent also shows a similar pattern in the Atlantic sector of the Arctic in the winter, suggesting the possibility of a role of the AMOC in the recent Arctic sea-ice decline in addition to anthropogenic greenhouse gas induced warming. However, in the summer, the simulated sea-ice response to the AMOC in the Pacific sector of the Arctic is much weaker than the observed declining trend, indicating a stronger role for other climate forcings or variability in the recently observed summer sea-ice decline in the Chukchi, Beaufort, East Siberian and Laptev Seas.

# 1. Introduction

Observations show an accelerating decline of the Arctic sea-ice cover (e.g Comiso et al. 2008; Kwok et al. 2009) and sea-ice thickness (Rothrock et al. 2008; Kwok and Rothrock 2009) in recent decades. While trends in the long term atmospheric circulation over the Arctic are not consistent with the declining trends in the Arctic sea-ice exhibited in the satellite record since 1979 (e.g. Deser and Teng 2008), the declining trends in the Arctic sea-ice have been found to be robustly linked to the rise in surface air temperature (SAT) over the Arctic in the past decades (e.g. Rothrock and Zhang 2005; Lindsay and Zhang 2005; Johannessen et al. 2004; Deser and Teng 2008). Whether the recent rapid Arctic warming is caused completely by enhanced anthropogenic greenhouse gas emissions (e.g. Johannessen et al. 2004; Zhang and Walsh 2006; Gillett et al. 2008; Moritz et al. 2002) or is amplified by low frequency oceanic variability (e.g. Bengtsson et al. 2004), is still a matter of debate.

Multi-model GCM ensemble-means indicate that only about half of the observed declining sea-ice cover trend is externally-forced in the 1979-2006 period, suggesting a strong role for natural variability in Arctic climate (Stroeve et al. 2007) provided that the simulated sensitivity of the Arctic sea ice to the external radiative forcing is approximately correct. On centennial time-scales, Polyakov et al. (2003) found that the limited data records of fast-ice thickness and extent in Kara, Laptev, East Siberian and Chukchi marginal seas lack a statistically significant long-term trend and are dominated by multidecadal/decadal oscillations over the 1900-2000 period.

The Atlantic Meridional Overturning Circulation (AMOC) is often thought to be a major source of decadal/multidecadal variability in the climate system (e.g. Delworth and Mann

2000; Polyakov et al. 2010). In coupled model simulations (e.g. Knight et al. 2005; Zhang 2008) the AMOC contributes a substantial fraction of the low-frequency variability of the basin averaged North Atlantic sea surface temperatures, i.e. the Atlantic Multidecadal Oscillation (AMO). The AMO has been linked to global and regional climate variability, such as the variability of Northern Hemisphere mean surface temperature (e.g. Zhang et al. 2007), Sahel drought (e.g. Folland et al. 1986), North American and western Europe summer climate (Sutton and Hodson 2005), Northeast Brazilian rainfall (e.g. Folland et al. 2001), Indian monsoon (e.g. Zhang and Delworth 2006), the Atlantic hurricane activities (Goldenberg et al. 2001) and recently Arctic SAT (Chylek et al. 2009). The focus of this study is to evaluate the impact of low frequency AMOC variability on the simulated Arctic SAT and sea-ice variations, in the absence of anthropogenic greenhouse gas induced warming, using a 1000 year-long segment of a control simulation of the GFDL coupled climate model CM2.1, (Delworth et al. 2006).

To compare the simulated impact of the AMOC on the Arctic sea-ice variations with the observed Arctic sea-ice data, we also analyze satellite-derived monthly sea-ice concentration data on a 25 km x 25 km grid for the period 1979-2008 obtained from National Snow and Ice Data Center (NSIDC) (Cavalieri et al. 1996, updated 2008). We also analyze a reconstructed sea-ice extent dataset over the Arctic from 1900-1999 (Zakharov 1997), and the Arctic SAT data derived from NANSEN SAT data provided by the Nansen Centers in St. Petersburg (Russia) and Bergen (Norway) (Kuzmina et al. 2008) to broadly benchmark the simulated Arctic sea-ice and SAT variability in the control simulation.

## 2. Simulated Arctic SAT and Sea-Ice Variability

In terms of annual mean Arctic-wide area averages, the simulated Arctic-averaged sea-ice and SAT variability in the 1000 year-long segment of the control run are broadly consistent with that of linearly detrended observations. The annual mean Arctic sea-ice extent and area-averaged SAT (northwards of 70°N) display a standard deviation of 0.15 million square kilometers and 0.57 K respectively for the last 100 years of the simulation. The linearly detrended century-long reconstructed sea-ice dataset (Zakharov 1997) and area averaged Arctic SAT dataset (Kuzmina et al. 2008) exhibit a standard deviation of 0.18 million square kilometers and 0.75 K respectively. The simulated sea-ice extent is defined as total marine areas with sea-ice concentrations greater than or equal to 15%. The results for observed sea-ice extent and SAT data show little sensitivity to linear or quadratic detrending.

The simulated annual mean Arctic SAT and sea-ice extent anomalies are also found to be significantly anti-correlated with each other (r = -0.96) on decadal time-scales when 10-year low-pass filtered (Figure 1a). The correlation between the two low-pass filtered time-series in the GFDL CM2.1 simulation is found to be statistically significant at the 95% confidence level for 71 degrees of freedom ($N_{effective} - 2$) based on a t-test. Filtering causes a loss of temporal degrees of freedom resulting in a smaller effective sample size, $N_{effective} = N/(1 + 2\Sigma_{i=1}^{N}\gamma_{1i}\gamma_{2i})$, where $N$ is the actual sample size and $\gamma_{1i}, \gamma_{2i}$ are the auto-correlations of the two filtered time-series at lag $i$, (Livezey and Chen 1983). The anti-correlation between detrended low-pass filtered timeseries of the observed Arctic sea-ice extent (Zakharov 1997) and Arctic SAT (Kuzmina et al. 2008) (r = -0.48, Figure 1b) is found to be lower than that found by Johannessen et al. (2004) (r = -0.6), who use a

different Arctic SAT dataset.

Figures 2a shows the spatial distribution of annual mean and fall, winter, spring and summer seasonal averages of Arctic sea-ice concentrations for the 1000-years control integration computed from monthly averaged data. We here denote the seasons of fall, winter, spring and summer as three month averages of November to January, February to April, May to July, and August to October respectively, based on the coherency of spatial pattern of sea-ice concentration in the individual months of each season, both in the observations and the control simulation. A similar definition of seasons was also used by Deser and Teng (2008) in their study of Arctic sea-ice. The annual and seasonal averages of the spatial distribution of the Arctic sea-ice concentration are also shown for the satellite-derived observations of the period 1979-2008 in Figure 2a. The spatial distribution of simulated Arctic sea-ice concentration climatology reveals the seasonal biases of GFDL CM2.1, with increased (decreased) southward extent in the winter (summer).

Figure 2b shows the inter-annual standard deviations of sea-ice concentrations over the Arctic Ocean for the GFDL CM2.1 control simulation and observations for different seasons. Notably, the variance of sea-ice concentrations is larger over the edge of the Arctic sea-ice cover in all months. The sea-ice cover edges contain thinner sea-ice with low sea-ice concentrations, which make the regions around the sea-ice edge volatile. The spatial structure of the simulated Arctic sea ice variability is broadly consistent with that observed. In the observed data, large variability is also seen in the Okhotsk Sea during the winter because of the presence of volatile sea-ice cover in the region. The fall and spring show slightly weaker variability as compared to the winter and summer seasons in both the GFDL CM2.1 model and the satellite-derived observations. Much of the Arctic sea ice variability in the

short satellite record is caused by the strong declining trend, thus the spatial pattern of observed sea-ice variability (Figure 2b) is found to be very similar to the spatial pattern of the observed trend (Figure 4e, Figure 6e).

# 3. Simulated Influence of the AMOC on the Arctic SAT and Sea Ice Variability

The GFDL CM2.1 control simulation shows pronounced low frequency AMOC variations with a period of 20 years (Zhang 2008; Msadek et al. 2010) and a standard deviation of 1.8 Sv. On decadal time-scales, the AMOC index is found to be significantly (at the 95% level) correlated and anti-correlated with the annual mean Arctic-averaged SAT (r = 0.39) and Arctic sea-ice extent (r = -0.4) respectively in the control simulation (Figure 3a, b), with the maximum correlation and anti-correlation occurring when the AMOC index leads by one year. The AMOC index is also found to be significantly correlated with the net upward surface heat flux (r = 0.47) released from the oceans to the atmosphere averaged over the sub-polar North Atlantic ocean (50°N-65°N) on decadal timescales (Figure 3c), and the maximum correlation occurs at zero time lag. Here, the AMOC index is defined as the maximum of the zonally integrated annual mean overturning streamfunction in the Atlantic at 40°N. Spatially, the strongest correlations/anti-correlations between the SAT/sea-ice and the AMOC index leading by one year are seen over the Labrador and Nordic Seas (Figure 3d, e), explaining about 40-60 %($r^2$) of the low-frequency variability of Arctic SAT and sea-ice concentrations in those regions. A regression of the net upward surface heat flux against

the AMOC index also reveals that an intensification of the AMOC is associated with an increased release of heat from the ocean to the atmosphere over the Labrador and Nordic Seas, peaking in the winter season (Figure 3f).

Figure 4a shows the composite of sea-ice extent both annually and seasonally averaged, when the value of the annual mean AMOC index (leading by one year) is greater (lesser) than a threshold of $2\sigma$ ($-2\sigma$), where $\sigma$ denotes the standard deviation of the AMOC index. Arctic sea-ice is found to retreat polewards as the AMOC intensifies in the control simulation. A linear regression of the low pass filtered Arctic SAT, sea-ice thickness and sea-ice concentration anomalies on the low-pass filtered standardized AMOC index (leading by one year) also suggests a connection between the low frequency Arctic sea-ice/SAT anomalies and the AMOC index in the Atlantic side of the Arctic throughout the year (Figure 4b-d). The Arctic warming and the reduction in sea-ice thickness/extent associated with an intensifying AMOC, are strengthened in the fall and strongest in the winter, and become much weaker in the spring and summer in the Labrador, Greenland and Barents Seas (Figure 4b-d).

An intensified AMOC also results in warming of the entire upper North Atlantic ocean, as indicated by the significant correlation between the AMOC index (leading by about two years) and the AMO index ($r = 0.65$, Figure 5a). The AMO index is defined as the area-averaged annual mean SST anomaly over the entire North Atlantic. The correlation coefficients of the Arctic SAT ($r = 0.56$) and Arctic sea-ice extent ($r = -0.57$) with the AMO index (Figure 5b, c) are found to be higher than those with the AMOC index directly (Figure 3a, b). The regression coefficients of Arctic anomalies against the AMO index (Figure 6) are also stronger than those against the AMOC index directly (Figure 4).

The coherent spatial patterns of the Arctic SAT and sea-ice concentration/thickness

associated with the AMOC in the fall and winter (Figure 4a-d) suggests that locally the SAT and sea-ice variations in the Arctic are coupled. In the control simulation, the stronger AMOC is associated with the stronger deep convection in the Labrador Sea and the Nordic Sea, thus larger amounts of heat released into the atmosphere there (Figure 3f) and over the entire sub-polar North Atlantic (Figure 3c), resulting in an increase in the SAT of the northern high latitudes. Also, in the Atlantic sector of the Arctic regions, warmer oceans associated with an intensified AMOC, would inhibit the formation of sea-ice in the freezing months starting from fall and into the winter. The ice-thickness feedback (e.g. Manabe and Stouffer 1980; Hall 2004) would strengthen the SAT, because the inhibited growth of sea-ice in the freezing period would lead to a reduced ice cover and formation of relatively thinner sea-ice starting in the fall, which also reduces the insulation of the cold winter atmosphere from the warmer ocean surface.

An intensification of the AMOC is associated with an increase in the upward surface long wave, sensible, and latent heat fluxes from the ocean to the atmosphere along with an increased net downward surface short wave heat flux into the ocean via the reduction in the surface albedo over the Labrador, Greenland and Barents Seas, in the fall and peaking in the winter (not shown). The increased net upward heat flux from the more open ocean surface (Figure 3c, f) as well as through the thinly ice-covered ocean to the atmosphere in the fall further increases the SAT and inhibits sea-ice formation in the winter (Figure 4d), leading to the largest decrease in sea-ice concentration and increase in Arctic SAT over the Labrador, Greenland and Barents Sea in March. In the lower latitudes of the Arctic most of the ocean is ice-free in the summer, and hence, in the absence of sea ice related feedbacks, the summer SAT anomaly is weakly associated with the AMOC variations there.

# 4. Comparison with the Observed Arctic Sea-Ice Concentration

Figure 4e shows the spatial distribution of the observed declining trend of the Arctic sea-ice concentration from 1979-2008. A significant declining trend in sea-ice concentrations is observed over the period 1979-2008 in the Labrador, Greenland, Barents and Okhotsk Seas in the fall and winter (Figure 4e). In the spring, a declining trend is observed in the Labrador, Barents Seas and the Pacific sector of the high latitude Arctic. The spatial pattern of the observed declining trend in the fall, winter and spring is similar to the spatial pattern of reduced sea-ice associated with an intensified AMOC and AMO in the GFDL CM2.1 control simulation in the Atlantic side of the Arctic, particularly the Labrador, Greenland and Barents Seas (Figure 4d, 6d). These similar spatial patterns suggest a possible role of the AMOC in the observed sea-ice declining trend in these regions over the recent decades in the fall, winter and spring.

In the summer, the observed sea-ice declining trend is strongest in the Chukchi, East Siberian and Laptev Seas in the Pacific sector of the Arctic. The simulated summer Arctic sea-ice decline associated with the AMOC is much weaker in these regions (Figure 4d,e), suggesting that the AMOC induced decadal/multidecadal natural variability has no direct contribution to the recent sea- ice decline in the Pacific sector of the Arctic. However, the standard deviation of modeled Arctic sea ice concentration from the control simulation does show a strong variability in the summer in these regions (Figure 2b). The results indicate that some other climate variability might play a role in the summer sea ice variability at the Pacific sector of the Arctic. Recent evidence also shows that the observed decline in the

Pacific sector of the Arctic sea-ice in the summer is caused by warming of the sub-surface Pacific summer waters with little direct contribution from warming in the Atlantic ocean (Shimada et al. 2006).

# 5. Discussion

A recent study suggests that the AMOC strength has increased in the past several decades (e.g. Zhang 2008). Our model results suggest that the strengthened AMOC, in addition to the anthropogenic greenhouse gas induced global warming, might have contributed to the observed declining trend in the winter sea-ice in Labrador and Nordic Seas in the past several decades. AMOC induced changes in the Arctic are, however, difficult to quantify. Our results from the GFDL CM2.1 model suggest that an increase of the AMOC of one standard deviation (1.8 Sv) could result in a decline in the winter sea ice in the Labrador and Nordic seas of similar magnitude as the observed decline trend per decade (Figure 4d, e). Statistical decadal forecast models constructed from AMOC fingerprints predict that the AMOC strength might decline in the next few years (e.g. Mahajan et al. 2011), which could potentially slowdown the rate of decline of the Arctic sea-ice in the Atlantic sector by partially offsetting the effects of the anthropogenic greenhouse gas induced global warming.

One caveat of this study is that the modeling results are based on one climate model (GFDL CM2.1), which shows seasonal biases in simulating the climatological mean Arctic sea ice. The accurate simulation of Arctic sea-ice remains a challenge for the climate modeling community, which is indicated by the large inter-model spread of Arctic sea-ice historical simulations and projections (Holland and Bitz 2003; Holland et al. 2010). It would be very

important to inter-compare results from different coupled climate models in future studies.

*Acknowledgments.*

We would like to thank Keith W. Dixon, John R. Lanzante, Michael Winton and three anonymous reviewers, whose suggestions and comments helped improve the manuscript. Mahajan S. was supported by the Visiting Scientist Program jointly sponsored by Princeton University and GFDL/NOAA.

# REFERENCES


Bengtsson, L., V. A. Semenov, and O. M. Johannessen, 2004: The early twentieth-century warming in the arctic- a possible mechanism. *Journal of Climate*, **17 (20)**, 4045–4057.

Chylek, P., C. K. Folland, G. Lesins, M. K. Dubey, and M. Wang, 2009: Arctic air temperature change amplification and the atlantic multidecadal oscillation. *Geophys. Res. Lett.*, **36**, L14 801.

Comiso, J. C., C. L. Parkinson, R. Gersten, and L. Stock, 2008: Accelerated decline in the arctic sea ice cover. *Geophys. Res. Lett.*, **35**, L01 703.

Delworth, T. L. and M. E. Mann, 2000: Observed and simulated multidecadal variability in the northern hemisphere. *Climate Dynamics*, **16 (9)**, 661–676.

Delworth, T. L., et al., 2006: Gfdl's cm2 global coupled climate models. part i: Formulation and simulation characteristics. *Journal of Climate*, **19 (5)**, 643–674.

Deser, C. and H. Teng, 2008: *Arctic Sea Ice Decline: Observations, Projections, Mechanisms, and Implications, Geophys. Monogr. Ser.*, Vol. 180, chap. Recent trends in Arctic sea ice and the evolving role of atmospheric circulation forcing, 1979-2007, 7–26. AGU.

Folland, C. K., A. W. Colman, D. P. Rowell, and M. K. Davey, 2001: Predictability of northeast brazil rainfall and real-time forecast skill, 1987-98. *Journal of Climate*, **14 (9)**, 1937–1958.

Folland, C. K., T. N. Palmer, and D. E. Parker, 1986: Sahel rainfall and worldwide sea temperatures, 1901-85. *Nature*, **320 (6063)**, 602–607.

Gillett, N. P., D. A. Stone, P. A. Stott, T. Nozawa, A. Y. Karpechko, G. C. Hegerl, M. F. Wehner, and P. D. Jones, 2008: Attribution of polar warming to human influence. *Nature Geosci*, **1 (11)**, 750–754.

Goldenberg, S. B., C. W. Landsea, A. M. Mestas-Nunez, and W. M. Gray, 2001: The recent increase in atlantic hurricane activity: Causes and implications. *Science*, **293 (5529)**, 474–479.

Hall, A., 2004: The role of surface albedo feedback in climate. *Journal of Climate*, **17 (7)**, 1550–1568.

Holland, M., M. Serreze, and J. Stroeve, 2010: The sea ice mass budget of the arctic and its future change as simulated by coupled climate models. *Climate Dynamics*, **34 (2)**, 185–200.

Holland, M. M. and C. M. Bitz, 2003: Polar amplification of climate change in coupled models. *Climate Dynamics*, **21 (3)**, 221–232.

Johannessen, O., et al., 2004: Arctic climate change: observed and modeled temperature and sea-ice variability. *Tellus A*, **56 (5)**, 559–560.

Knight, J. R., R. J. Allan, C. K. Folland, M. Vellinga, and M. E. Mann, 2005: A signature of persistent natural thermohaline circulation cycles in observed climate. *Geophys. Res. Lett.*, **32**, L020 708.

Kuzmina, S. I., O. M. Johannessen, L. Bengtsson, O. G. Aniskina, and L. Bobylev, 2008: High northern latitude surface air temperature: comparison of existing data and creation of a new gridded data set 1900–2000. *Tellus A*, **60 (2)**, 289–304.

Kwok, R., G. F. Cunningham, M. Wensnahan, I. Rigor, H. J. Zwally, and D. Yi, 2009: Thinning and volume loss of the arctic ocean sea ice cover: 2003–2008. *J. Geophys. Res.*, **114**, C07 005.

Kwok, R. and D. A. Rothrock, 2009: Decline in arctic sea ice thickness from submarine and icesat records: 1958–2008. *Geophys. Res. Lett.*, **36**, L15 501.

Lindsay, R. W. and J. Zhang, 2005: The thinning of arctic sea ice, 1988-2003: Have we passed a tipping point? *Journal of Climate*, **18 (22)**, 4879–4894.

Livezey, R. E. and W. Y. Chen, 1983: Statistical field significance and its determination by monte carlo techniques. *Monthly Weather Review*, **111 (1)**, 46–59.

Mahajan, S., R. Zhang, T. L. Delworth, S. Zhang, A. J. Rosati, and Y.-S. Chang, 2011: Predicting atlantic meridional overturning circulation (amoc) variations using subsurface and surface fingerprints. *Deep Sea Research II (in press)*.

Manabe, S. and R. J. Stouffer, 1980: Sensitivity of a global climate model to an increase of co2 concentration in the atmosphere. *J. Geophys. Res.*, **85**, 5529–5554.

Moritz, R. E., C. M. Bitz, and E. J. Steig, 2002: Dynamics of recent climate change in the arctic. *Science*, **297 (5586)**, 1497–1502.

Msadek, R., K. W. Dixon, T. L. Delworth, and W. Hurlin, 2010: Assessing the predictability

of the atlantic meridional overturning circulation and associated fingerprints. *Geophys. Res. Lett.*, **37 (19)**, L19 608.

Polyakov, I., V. Alexeev, U. Bhatt, E. Polyakova, and X. Zhang, 2010: North atlantic warming: patterns of long-term trend and multidecadal variability. *Climate Dynamics*, **34 (2)**, 439–457.

Polyakov, I. V., et al., 2003: Long-term ice variability in arctic marginal seas. *Journal of Climate*, **16 (12)**, 2078–2085.

Rothrock, D. A., D. B. Percival, and M. Wensnahan, 2008: The decline in arctic sea-ice thickness: Separating the spatial, annual, and interannual variability in a quarter century of submarine data. *J. Geophys. Res.*, **113**, –.

Rothrock, D. A. and J. Zhang, 2005: Arctic ocean sea ice volume: What explains its recent depletion? *J. Geophys. Res.*, **110**, C01 002.

Shimada, K., T. Kamoshida, M. Itoh, S. Nishino, E. Carmack, F. McLaughlin, S. Zimmermann, and A. Proshutinsky, 2006: Pacific ocean inflow: Influence on catastrophic reduction of sea ice cover in the arctic ocean. *Geophys. Res. Lett.*, **33**, L08 605.

Stroeve, J., M. M. Holland, W. Meier, T. Scambos, and M. Serreze, 2007: Arctic sea ice decline: Faster than forecast. *Geophys. Res. Lett.*, **34**, L09 501.

Sutton, R. T. and D. L. R. Hodson, 2005: Atlantic ocean forcing of north american and european summer climate. *Science*, **309 (5731)**, 115–118.

Zakharov, V. F., 1997: Sea ice in the climate system. *World Climate Research Programme/ Arctic Climate System Study, WMO/TD 782*, World Meteorological Organization, Geneva, 80 pp.

Zhang, R., 2008: Coherent surface-subsurface fingerprint of the atlantic meridional overturning circulation. *Geophys. Res. Lett.*, **35**, L20 705.

Zhang, R. and T. L. Delworth, 2006: Impact of atlantic multidecadal oscillations on india/sahel rainfall and atlantic hurricanes. *Geophys. Res. Lett.*, **33**, L23 708.

Zhang, R., T. L. Delworth, and I. M. Held, 2007: Can the atlantic ocean drive the observed multidecadal variability in northern hemisphere mean temperature? *Geophys. Res. Lett.*, **34**, L02 709.

Zhang, X. and J. E. Walsh, 2006: Toward a seasonally ice-covered arctic ocean: Scenarios from the ipcc ar4 model simulations. *Journal of Climate*, **19 (9)**, 1730–1747.

# List of Figures

3 Time series and correlation/regression maps from the 1000-year long segment of the GFDL CM2.1 simulation. (a) 10-year LP filtered and standardized annual mean Arctic area-averaged SAT and AMOC index. (b) 10-year LP filtered and standardized annual mean Arctic sea-ice extent and AMOC index. The maximum correlation between Arctic SAT and AMOC (r = 0.39) and the maximum anti-correlation between Arctic sea-ice extent and AMOC (r = -0.4) occur when the AMOC leads by one year. (c) 10-year LP filtered and standardized winter (FMA) net surface heat flux over the sub-polar North Atlantic ocean (50°N-65°N) and AMOC index. (d) Correlation map of 10-year LP filtered annual mean Arctic SAT with the LP filtered AMOC index which leads by one year. (e) Same as (d), but for Arctic sea-ice concentration. Line contours indicate regions where the correlation coefficient is statistically significant at the 95% level based on a t-test. (f) Regression map of LP filtered winter (FMA) net surface heat flux against the LP filtered AMOC index. Positive values correspond to upward surface heat flux. 23

4 Composite and regression maps with respect to the AMOC index. (a) Composite of annual, fall (NDJ), winter (FMA), spring (MJJ) and summer (ASO) sea-ice extent when the AMOC index (leading by one year) crosses the threshold of twice its standard deviation for the 1000-year segment of the control simulation. Blue Shading (red shading) represents the sea-ice extent when AMOC index is positive (negative). (b)-(d) Regression of low pass filtered annual, fall, winter, spring and summer Arctic SAT, sea-ice thickness and concentration on standardized low pass filtered AMOC index which leads by one year for the 1000-year segment of the control simulation. (e) Linear trend (per decade) of observed Arctic sea-ice concentration from 1979-2008. Note that red shades indicate negative values in (c)-(e). 24

5 Annual mean time series from the 1000-year long segment of the GFDL CM2.1 control simulation. (a) 10-year LP filtered and standardized AMO index and AMOC anomalies (the maximum correlation between AMO index and AMOC index occurs when the AMOC index leads by about two years (r = 0.65), (b) Arctic area-averaged SAT and AMO index and (c) Arctic sea-ice extent and AMO index. 25

6 Composite and regression maps with respect to the AMO index. (a) Composite of annual, fall (NDJ), winter (FMA), spring (MJJ) and summer (ASO) sea-ice extent when the AMO index crosses the threshold of twice its standard deviation for the 1000-year segment of the control simulation. Blue shading (red shading) represents the sea-ice extent when AMO is positive (negative). (b)-(d) Regression of LP filtered annual, fall, winter, spring and summer Arctic SAT, sea-ice thickness and concentration on standardized LP filtered AMO index for the 1000-year segment of the control simulation. (e) Linear trend (per decade) of observed Arctic sea-ice concentration from 1979-2008 (same as Figure 4e). Note that red shades indicate negative values in (c)-(e). 26

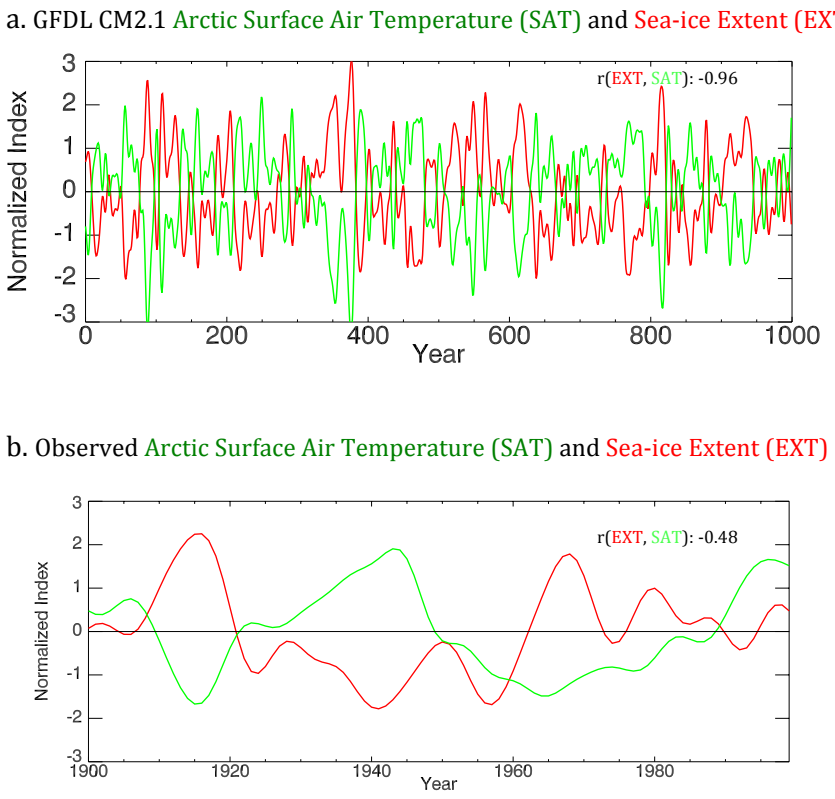


FIG. 1. 10-year low pass (LP) filtered and standardized (zero mean, unit standard deviation) timeseries of Arctic area-averaged surface air temperature (SAT, green) and Arctic sea-ice extent (EXT, red) of the (a) 1000-year long segment of the GFDL CM2.1 control simulation and (b) detrended observations for the period 1900-1999 ( NANSEN SAT data (green) and Zakharov sea-ice dataset (red)).

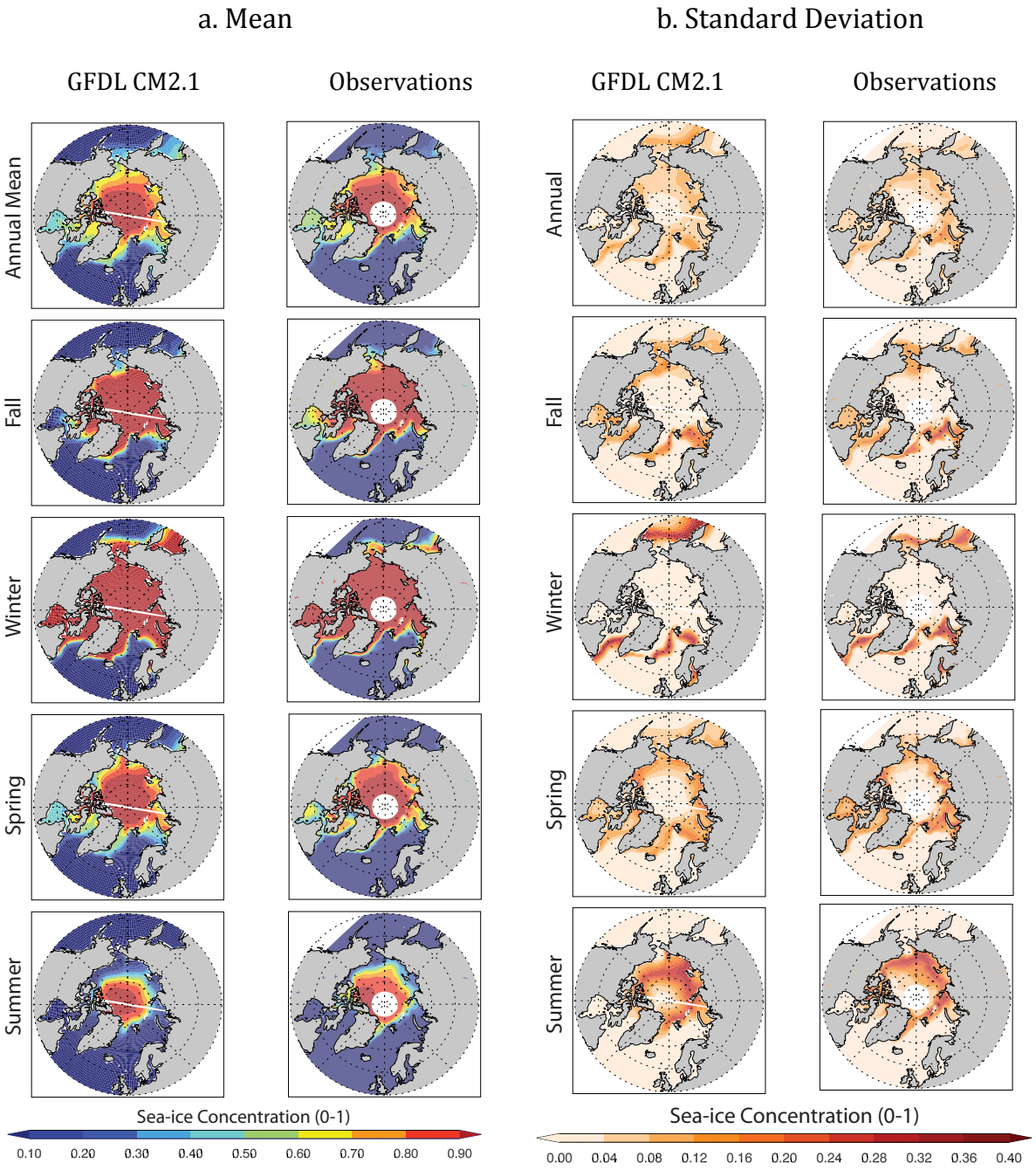


FIG. 2. Climatological mean and standard deviation of modeled and observed Arctic sea-ice concentration. (a) Climatological mean of annual, fall (NDJ), winter (FMA), spring (MJJ) and summer (ASO) sea-ice concentration in the 1000-year segment of the control simulation and satellite observations from 1979-2008. (b) Standard deviation of annual, fall (NDJ), winter (FMA), spring (MJJ) and summer (ASO) sea-ice concentration in the 1000-year segment of the control simulation and satellite observations from 1979-2008.

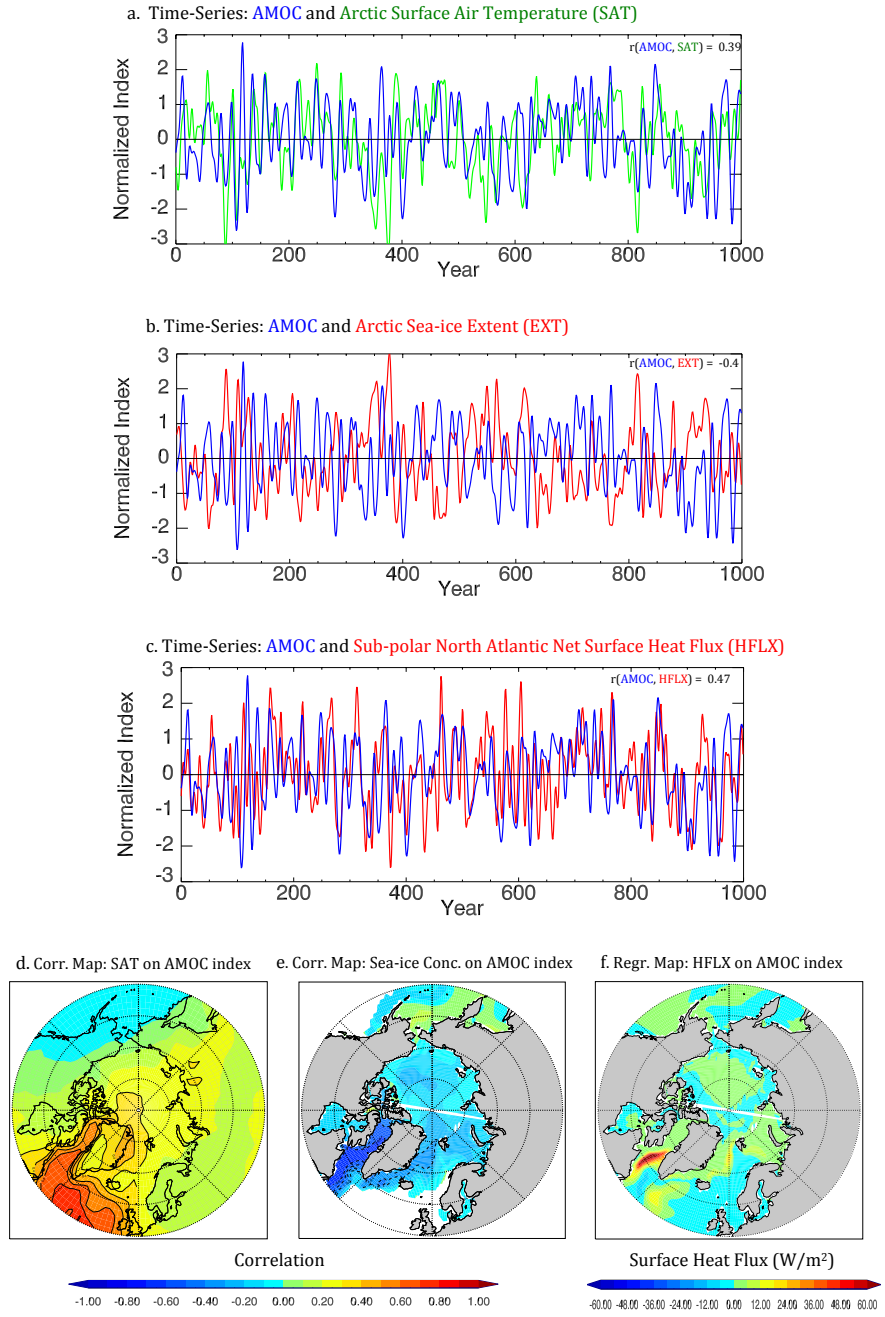


FIG. 3. Time series and correlation/regression maps from the 1000-year long segment of the GFDL CM2.1 simulation. (a) 10-year LP filtered and standardized annual mean Arctic area-averaged SAT and AMOC index. (b) 10-year LP filtered and standardized annual mean Arctic sea-ice extent and AMOC index. The maximum correlation between Arctic SAT and AMOC (r = 0.39) and the maximum anti-correlation between Arctic sea-ice extent and AMOC (r = -0.4) occur when the AMOC leads by one year. (c) 10-year LP filtered and standardized winter (FMA) net surface heat flux over the sub-polar North Atlantic ocean (50°N-65°N) and AMOC index. (d) Correlation map of 10-year LP filtered annual mean Arctic SAT with the LP filtered AMOC index which leads by one year. (e) Same as (d), but for Arctic sea-ice concentration. Line contours indicate regions where the correlation coefficient is statistically significant at the 95% level based on a t-test. (f) Regression map of LP filtered winter (FMA) net surface heat flux against the LP filtered AMOC index. Positive values correspond to upward surface heat flux.

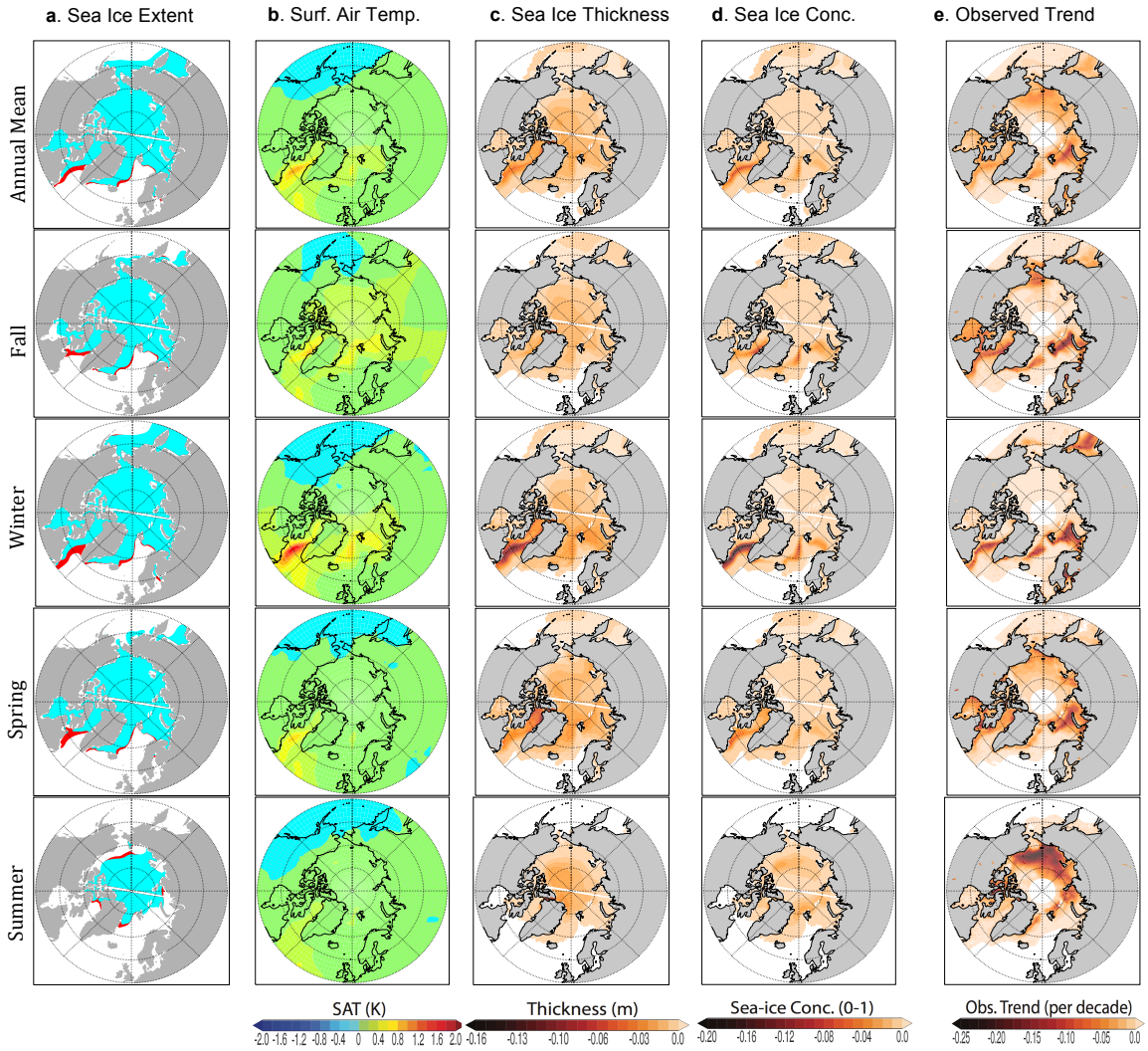


FIG. 4. Composite and regression maps with respect to the AMOC index. (a) Composite of annual, fall (NDJ), winter (FMA), spring (MJJ) and summer (ASO) sea-ice extent when the AMOC index (leading by one year) crosses the threshold of twice its standard deviation for the 1000-year segment of the control simulation. Blue Shading (red shading) represents the sea-ice extent when AMOC index is positive (negative). (b)-(d) Regression of low pass filtered annual, fall, winter, spring and summer Arctic SAT, sea-ice thickness and concentration on standardized low pass filtered AMOC index which leads by one year for the 1000-year segment of the control simulation. (e) Linear trend (per decade) of observed Arctic sea-ice concentration from 1979-2008. Note that red shades indicate negative values in (c)-(e).

a. Time-series: AMO index and AMOC index

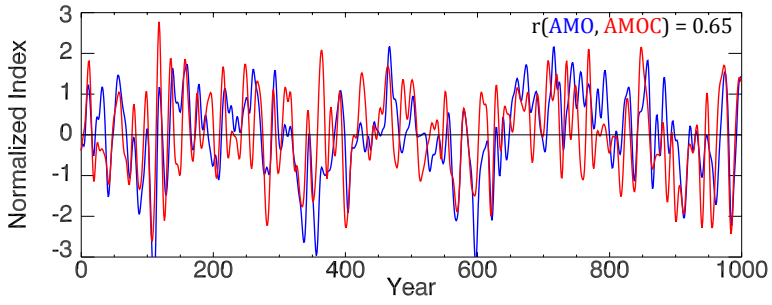


b. Time-series: AMO index and Arctic Surface Air Temperature (SAT)

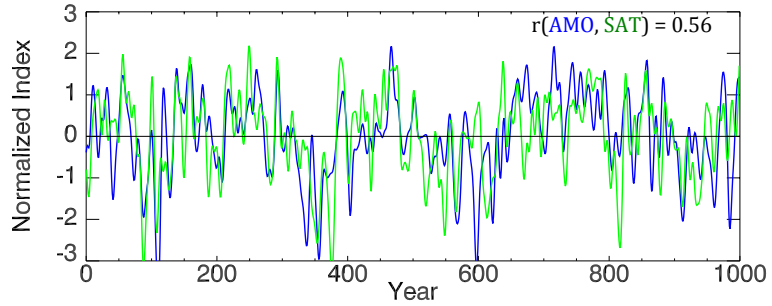


c. Time-series: AMO index and Arctic sea-ice extent (EXT)

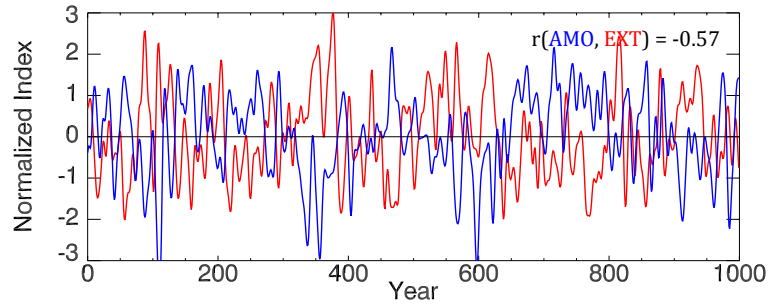


FIG. 5. Annual mean time series from the 1000-year long segment of the GFDL CM2.1 control simulation. (a) 10-year LP filtered and standardized AMO index and AMOC anomalies (the maximum correlation between AMO index and AMOC index occurs when the AMOC index leads by about two years (r = 0.65), (b) Arctic area-averaged SAT and AMO index and (c) Arctic sea-ice extent and AMO index.

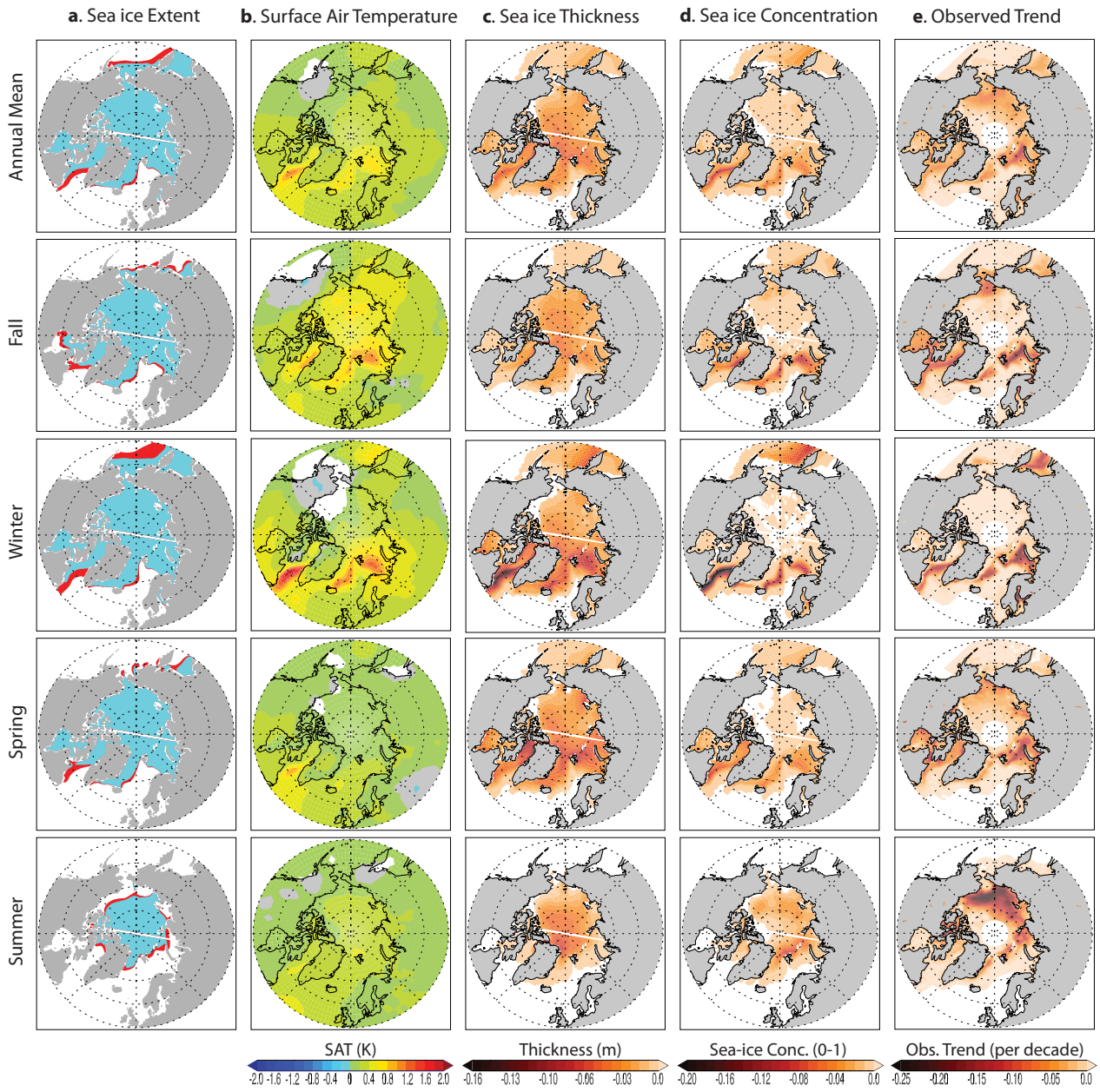


FIG. 6. Composite and regression maps with respect to the AMO index. (a) Composite of annual, fall (NDJ), winter (FMA), spring (MJJ) and summer (ASO) sea-ice extent when the AMO index crosses the threshold of twice its standard deviation for the 1000-year segment of the control simulation. Blue shading (red shading) represents the sea-ice extent when AMO is positive (negative). (b)-(d) Regression of LP filtered annual, fall, winter, spring and summer Arctic SAT, sea-ice thickness and concentration on standardized LP filtered AMO index for the 1000-year segment of the control simulation. (e) Linear trend (per decade) of observed Arctic sea-ice concentration from 1979-2008 (same as Figure 4e). Note that red shades indicate negative values in (c)-(e).